Electronic Supplementary Material (ESI) for Journal of Materials Chemistry C.

High-Performance non-doped blue OLEDs based on 1,2,4-triazole-phenanthroimidazole derivatives with negligible efficiency roll-off

Wenjuan Cao, Alim Abdurahman, Ping Zheng, Ming Zhang*, Feng Li

State Key Laboratory of Supramolecular Structure and Materials, College of Chemistry, Jilin University, Qianjin Avenue 2699, Changchun, 130012, P. R. China

*E-mail: zhming@jlu.edu.cn

Contents

1. Synthesis
2. Thermal stability and electrochemical properties
3. Lippert-Mataga calculation
4. The transient PL decay
5. The fluorescence and phosphorescence spectra
6. Theoretical Calculations
7. Electroluminescence Performances
8. EL spectra of OLEDs at different voltages
9. Luminescence -current density characteristics
10. Spectra data

1. Synthesis

General information

All reagents and solvents required for synthesis and characterization are purchased from commercial suppliers and used directly without any treatment. A Bruker Avance-III 500 and 600 NMR spectrometer was used for the ^{1}H and ^{13}C NMR data collection in $CDCl_3$ and DMSO solvent with tetramethylsilane as the internal standard. Mass spectra of all compounds were recorded on Thermo Fisher ITQ1100 GC-MS mass detector. A shimadzu UV-2550 spectrophotometer was applied to record the ultraviolet (UV)-visible spectra. Fluorescence spectra were recorded using a RF-5301 PC spectrophotometer. The electrochemical oxidation and reduction potentials were recorded using an electrochemical analyzer (CHI660C, CH Instruments, USA). The fluorescence decay spectra were recorded on an Edinburgh fluorescence spectrometer (FLS980), and the lifetime of the excited states was measured by the time-correlated single photon counting method under the excitation of a laser (375 nm). Thermal gravimetric analysis (TGA) were characterized by a TA INSTRUMENTS Q500 TGA analyzer. Differential scanning calorimetry (DSC) was measured on a Netzsch DSC204 instrument at a heating rate of 10℃ min^{-1} from 20℃ to 400℃ under nitrogen flushing.

Synthesis

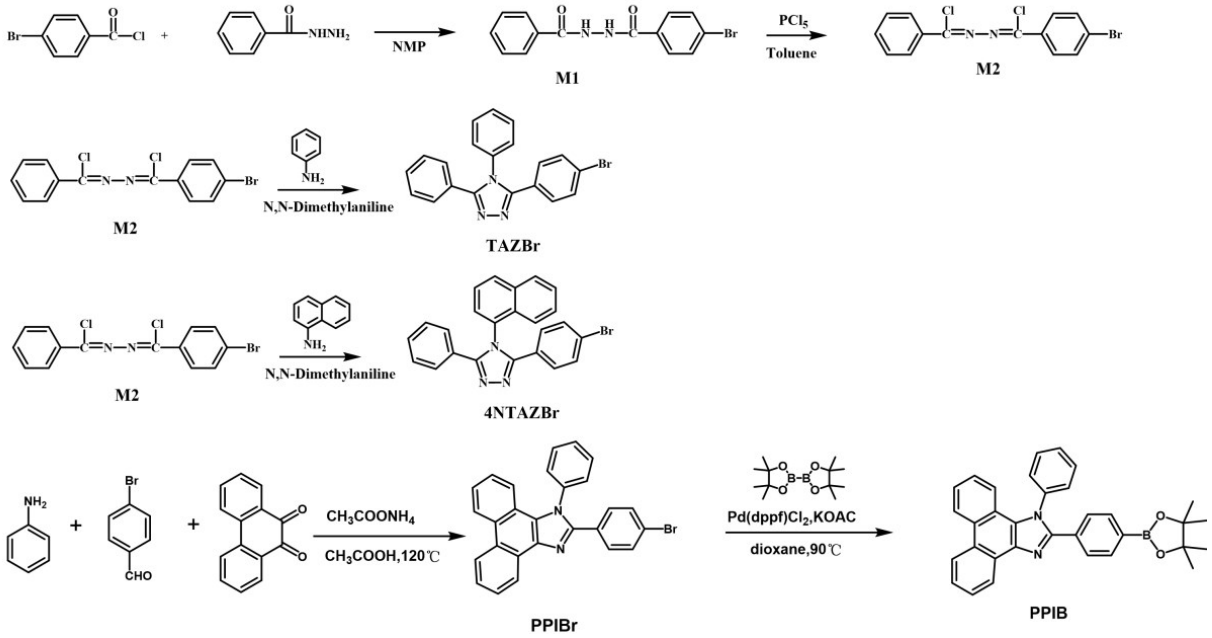

Scheme 1. Synthetic routes and chemical structures of TAZBr, 4NTAZBr and PPIB.

Synthesis of N'-benzoyl-4-bromobenzohydrazide (M1)

Under an argon atmosphere, 4-Bromobenzoic chloride (10.5 g, 47.7 mmol), Benzamide (4.5 g, 36.7 mmol), and 100 ml of N-methylpyrrolidone (NMP) were placed in a 250 ml round-bottom flask. Reaction at 0 °C for 1h, stir at room temperature for 12 hours. The mixture was stirred at room temperature for 12 h, poured into a large amount of distilled water. The appearing precipitates were collected by filtration. Washed with water and methyl alcohol and then dried to afford M1 (10.18g. yield: 87.1%), δ 10.62 (s, 1H), 10.54 (s, 1H), 7.98 – 7.91 (m, 2H), 7.91 – 7.83 (m, 2H), 7.77 (d, *J* = 8.5 Hz, 2H), 7.61 (t, *J* = 7.4 Hz, 1H), 7.54 (t, *J* = 7.5 Hz, 2H). MS (m/z) calculated for $C_{14}H_{11}BrN_2O_2$：318; Found $[M]^+$ 318.53.

Synthesis of 4-bromo-N-(chloro(phenyl)methylene)benzohydrazonoyl chloride (M2)

M1 (5.0 g, 15.7 mmol) and toluene (100 mL) were added into a 250 mL of two-necked round-bottom flask equipped with a reflux condenser. PCl_5 (7.5 g, 36.1 mmol)

was added under an argon atmosphere. The mixture was stirred at 120 °C for 4 h and then cooled to room temperature. 50 mL deionized water was added to the mixture then extracted with dichloromethane for several times. The solid was dried under reduced pressure and further purified by silica gel column chromatography using the Petroleum ether/dichloromethane (5:1, v/v) mixture as the eluent. A yellow-green powder was obtained (4.4g, yield: 67.2%) ^{1}H NMR (500 MHz, DMSO) δ 8.12-8.05 (m, 2H), 8.04-7.99 (m, 2H), 7.86-7.79 (m, 2H), 7.68(t, *J* = 7.4 Hz, 1H), 7.61 (dd, *J* = 10.5 Hz, 2H). MS (m/z) calculated for $C_{14}H_9BrN_2Cl_2$： 355.93; Found $[M]^+$ 355.76.

Synthesis of 3-(4-bromophenyl)-4,5-diphenyl-4*H*-1,2,4-triazole (TAZBr)

The mixture of M2 (3.0 g, 8.4 mmol), aniline (2.0 g, 21.0 mmol), and 40 mL of N,N-dimethylaniline was stirred at 135°C for 12 h under argon atmosphere. Add 30 mL of 2 M HCl (aq), the mixture was stirred for another 1 h. The precipitated solids were collected by filtration, dried and then purified by silica gel column chromatography using the dichloromethane/ethyl acetate (3:1, v/v) mixture as the eluent. A white powder was obtained (1.9g, yield: 60.1%).^{1}H NMR (500 MHz, DMSO) δ 7.61-7.57 (m, 2H), 7.54-7.46 (m, 3H), 7.46-7.31 (m, 9H).MS (m/z) calculated for $C_{20}H_{14}BrN_3$： 375.04; Found $[M]^+$ 375.87.

Synthesis of 3-(4-bromophenyl)-4-(naphthalen-1-yl)-5-phenyl-4*H*-1,2,4-triazole (4NTAZBr)

4NTAZBr was synthesized with the same method as compound TAZBr. A white powder was obtained (1.8g, yield: 51.3%).^{1}H NMR (500 MHz, DMSO) δ 8.18 (d, *J* = 8.3 Hz, 1H), 8.09 (d, *J* = 8.2 Hz, 1H), 7.98 (d, J = 7.2 Hz, 1H), 7.69 (t, *J* = 7.8 Hz, 1H),

7.59 (t, J = 7.4 Hz, 1H), 7.52 (m, 3H), 7.37 (m, 2H), 7.33 (t, J = 7.7 Hz, 3H), 7.27 (t, J = 7.5 Hz, 2H), 7.19 (d, J = 8.4 Hz, 1H). MS (m/z) calculated for $C_{24}H_{16}BrN_3$： 425.05; Found $[M]^+$ 426.15.

2. Thermal stability and electrochemical properties

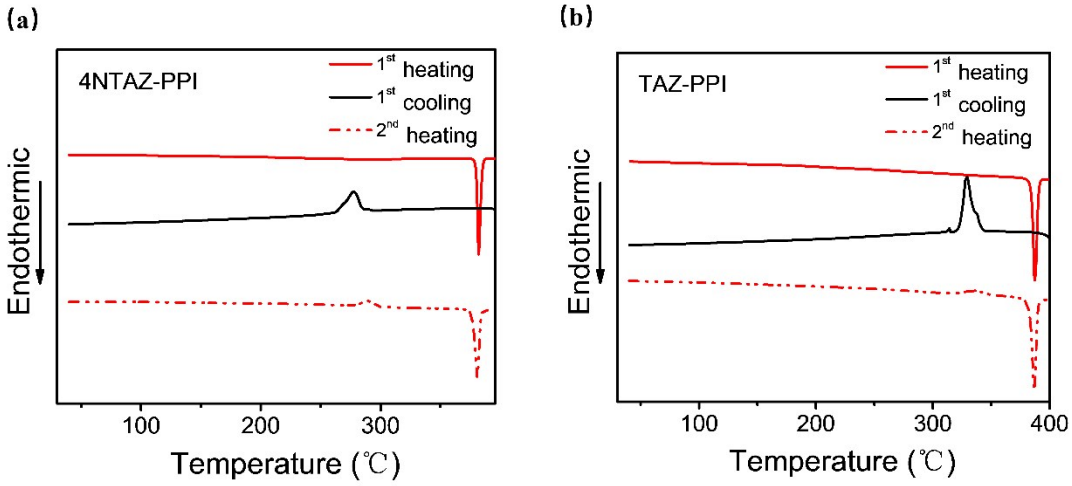

Figure S1. DSC curves of (a) 4NTAZ-PPI and (b)TAZ-PPI.

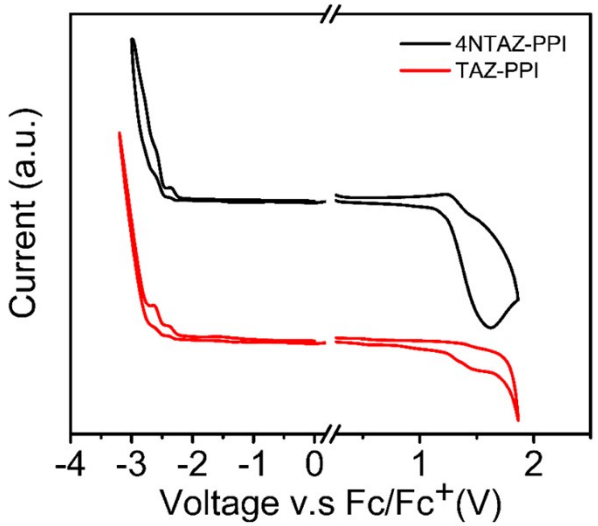

Figure S2. The electrochemical CV curves for 4NTAZ-PPI and TAZ-PPI. The oxidation and reduction potentials were measured in DCM and DMF solutions, respectively.

3. Lippert-Mataga calculation

To further understand the effect of solvent polarity on the excited state of 4NTAZ-PPI and TAZ-PPI, we used the Lippert-Mataga equation, a model that describes the interactions between the solvent and the dipole moment of solute:

$$hc(\nu_a - \nu_f) = hc(\nu_a^0 - \nu_f^0) + \frac{2(\mu_e - \mu_g)^2}{a_0^3} f(\varepsilon, n)$$

where f is the orientational polarizability of the solvent, $(\nu_a^0 - \nu_f^0)$ corresponds to the Stokes shifts when f is zero; μ_e is the excited state dipole moment; μ_g is the ground-state dipole moment (estimated to be 3.7 D for 4NTAZ-PPI and 2.9 D for TAZ-PPI using DFT calculations, respectively); a_0 is the solvent cavity (Onsager) radius, derived from the Avogadro number (N), molecular weight (M), and density (d=1.0 g/cm^3); ε and n are the solvent dielectric and the solvent refractive index, respectively; $f(\varepsilon,n)$ and a can be calculated respectively as follows:

$$f(\varepsilon, n) = \left[\frac{\varepsilon - 1}{2\varepsilon + 1} - \frac{n^2 - 1}{2n^2 + 1}\right], \quad a = \left(\frac{3M}{4N\pi d}\right)^{\frac{1}{3}}$$

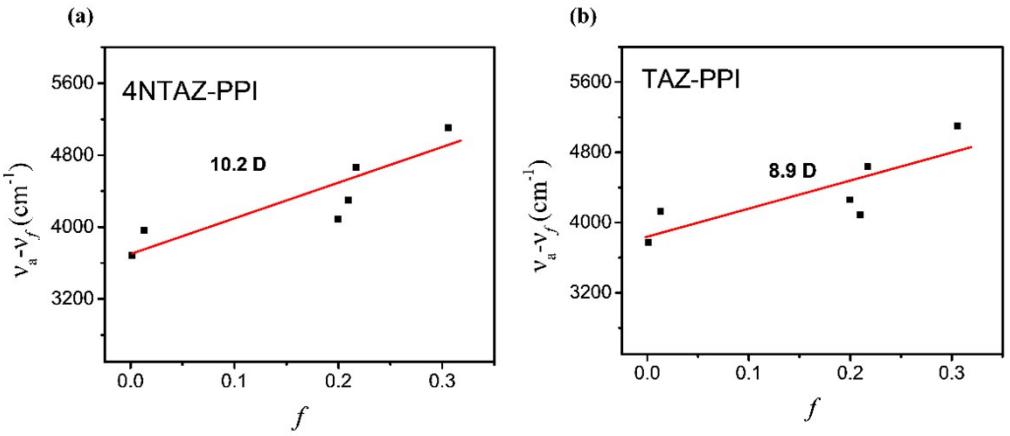

Figure S3. The plot of the Stokes shifts $(\nu_a - \nu_f)$ versus the solvent polarity function (f) for (a) 4NTAZ-PPI and (b) TAZ-PPI.

4. The transient PLdecay

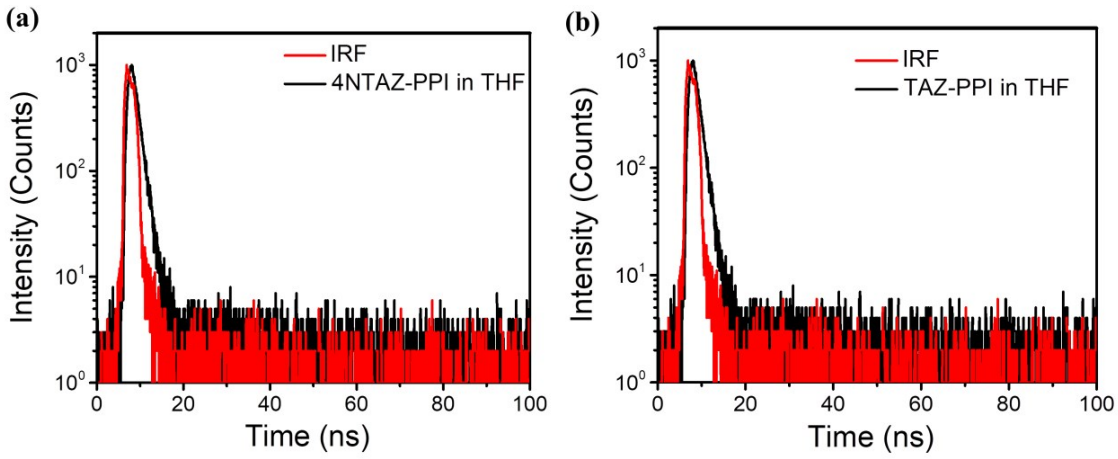

Figure S4. The transient PL decay in THF solution at room temperature (a) 4NTAZ-PPI and (b) TAZ-PPI in dilute THF solution

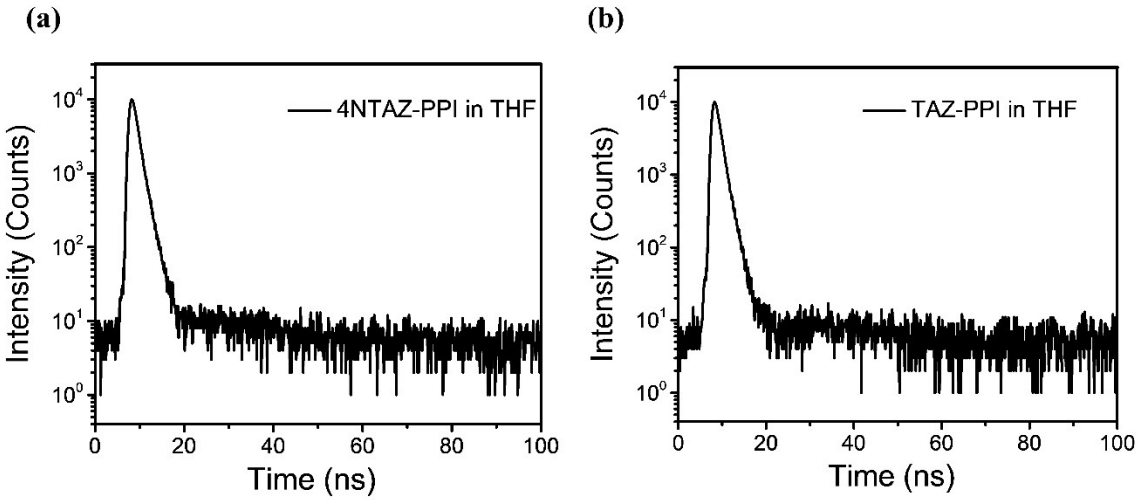

Figure S5. The transient PL decay of the(a) 4NTAZ-PPI and (b) TAZ-PPI in dilute THF solution at a temperature of 77 K.

5. The fluorescence and phosphorescence spectra

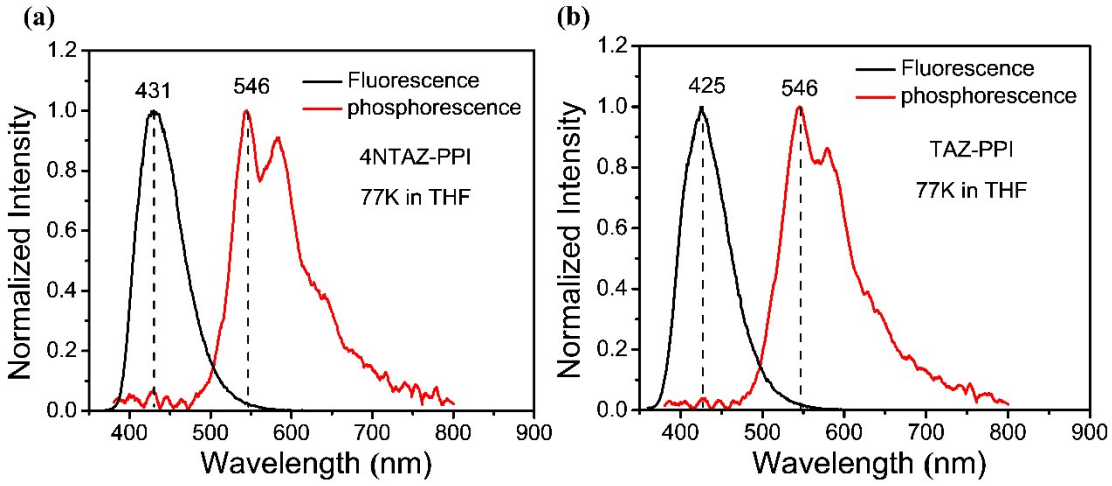

Figure S6. The fluorescence (at 77 K) and phosphorescence (at 77 K) spectra of (a) 4NTAZ-PPI and (b) TAZ-PPI in dilute THF.

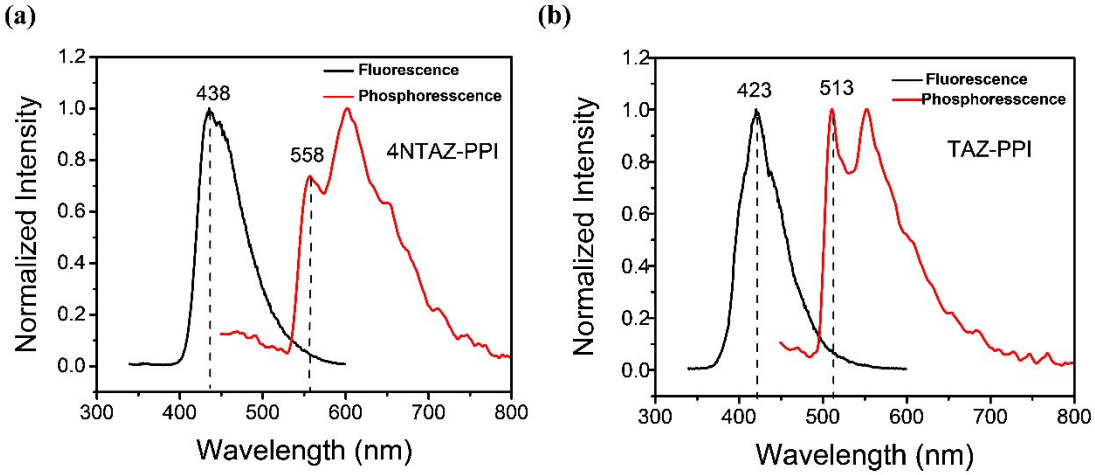

Figure S7. The fluorescence (at 77 K) and phosphorescence (at 77 K) spectra of (a) 4NTAZ-PPI and (b) TAZ-PPI spin-coating pristine films.

6. Theoretical calculations

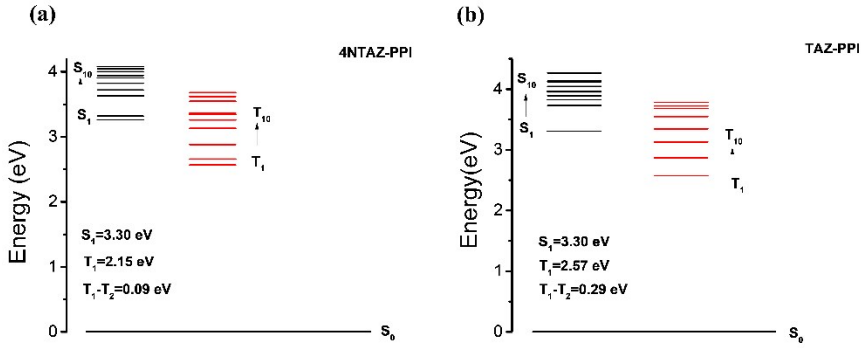

Figure S8. The energy landscape for singlet and triplet excited states. (Time dependent DFT calculation using the b3lyp/6-31g (d, p) method.)

7. Electroluminescence Performances

To assess the transporting properties of TAZ-PPI and 4NTAZ-PPI, single-carrier devices were fabricated with structure of ITO/MoO_3(10 nm)/TAZ-PPI or 4NTAZ-PPI(80nm)/MoO_3(10 nm)/Al(100 nm) for hole-only device and ITO/Al(100 nm)/LiF(1 nm)/4NTAZ-PPI or TAZ-PPI(80 nm)/LiF(1 nm)/Al(100 nm) for electron-only device. The calculation formulas for carrier mobility (μ) are expressed as following list:

$$J = \frac{9}{8}\varepsilon\varepsilon_0\mu\frac{V^2}{d^3}$$

Where ε is the relative permittivity; ε_0 is the free space permittivity (8.85 ×10^{-14}C/V cm); V is the effective voltage applied to the device and d is the thickness of the organic layer. μ is carrier mobility.

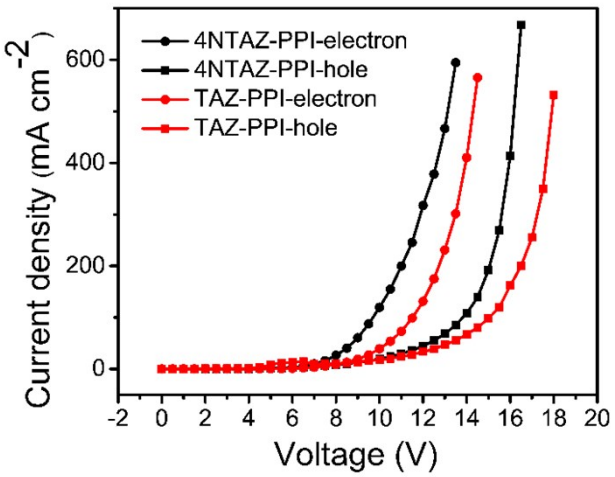

Figure S9. Current density-voltage characteristics of the hole-only devices (HOD) and electron-only devices (EOD).

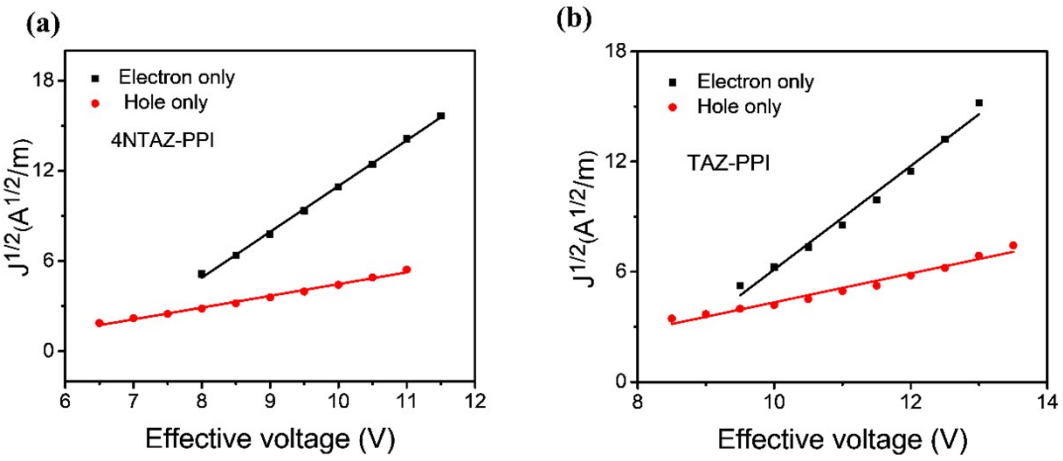

Figure S10. The $J^{1/2}$-V curves of single-carrier devices at the space-charge limited current district. (a) 4NTAZ-PPI and (b) TAZ-PPI.

8. EL spectra of OLEDs at different voltages

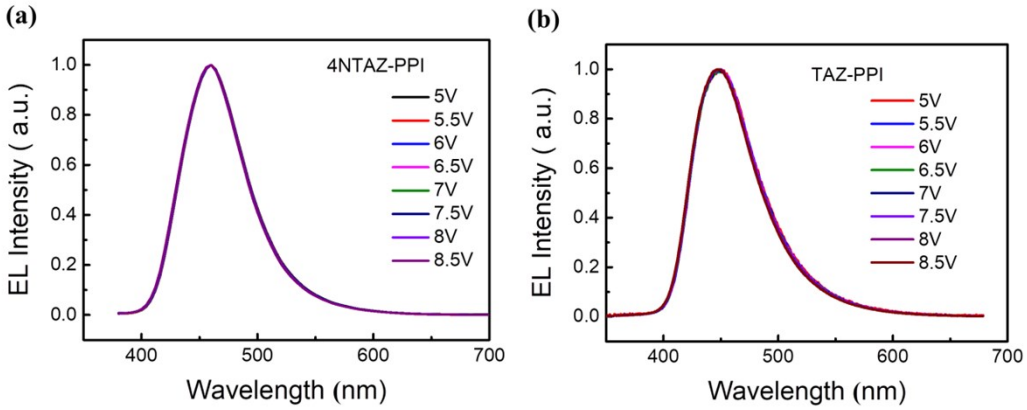

Figure S11. The EL spectrum of (a) 4NTAZ-PPI and (b) TAZ-PPI.

9. Luminescence -current density characteristics

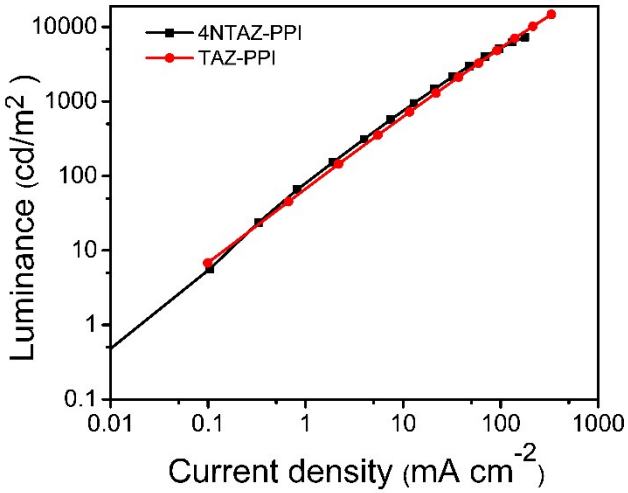

Figure S12. Luminance-current density characteristics of 4NTAZ-PPI and TAZ-PPI

10. Spectra data

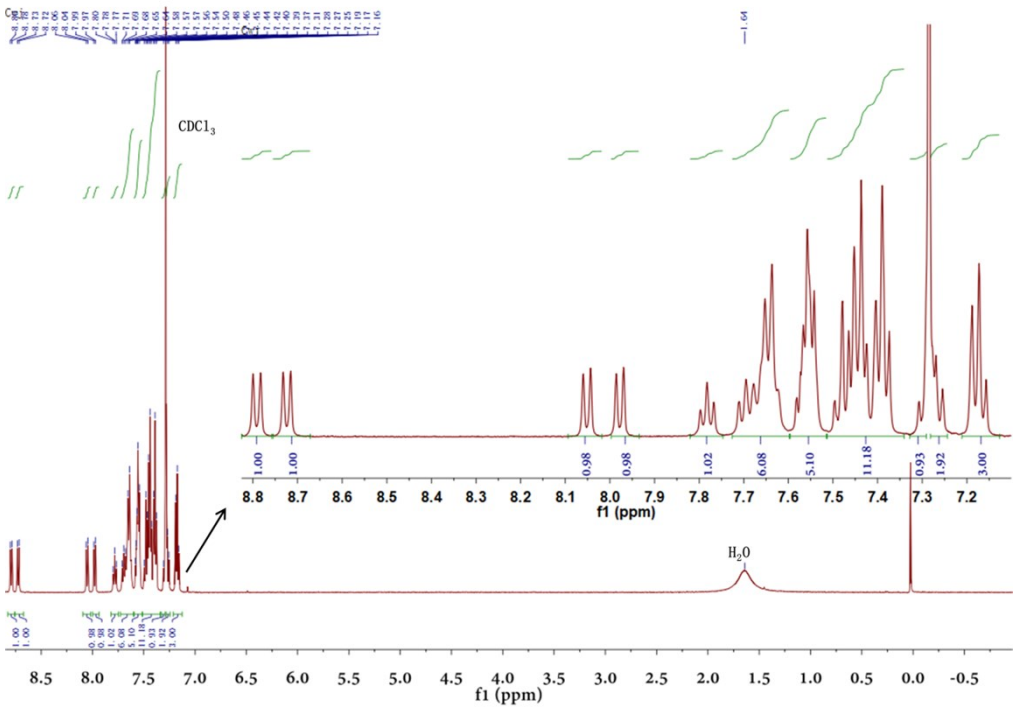

Figure S13. ^{1}H NMR spectrum of 4NTAZ-PPI in $CDCl_3$.

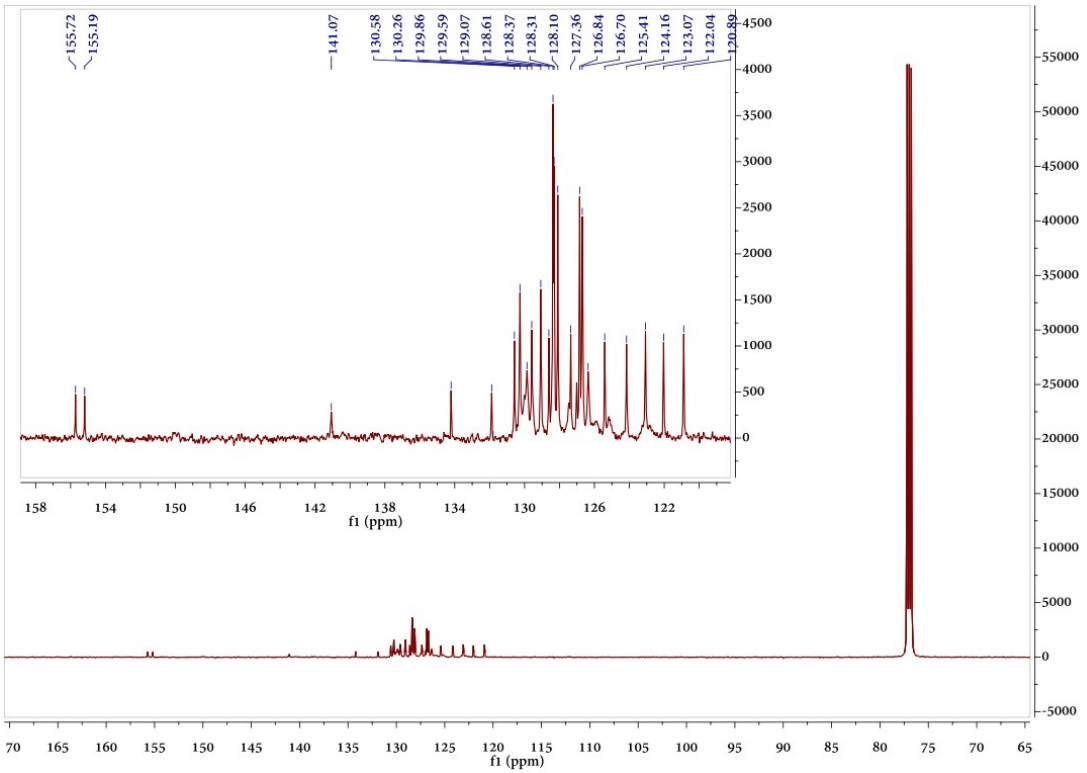

Figure S14. ^{13}C NMR spectrum of 4NTAZ-PPI in $CDCl_3$.

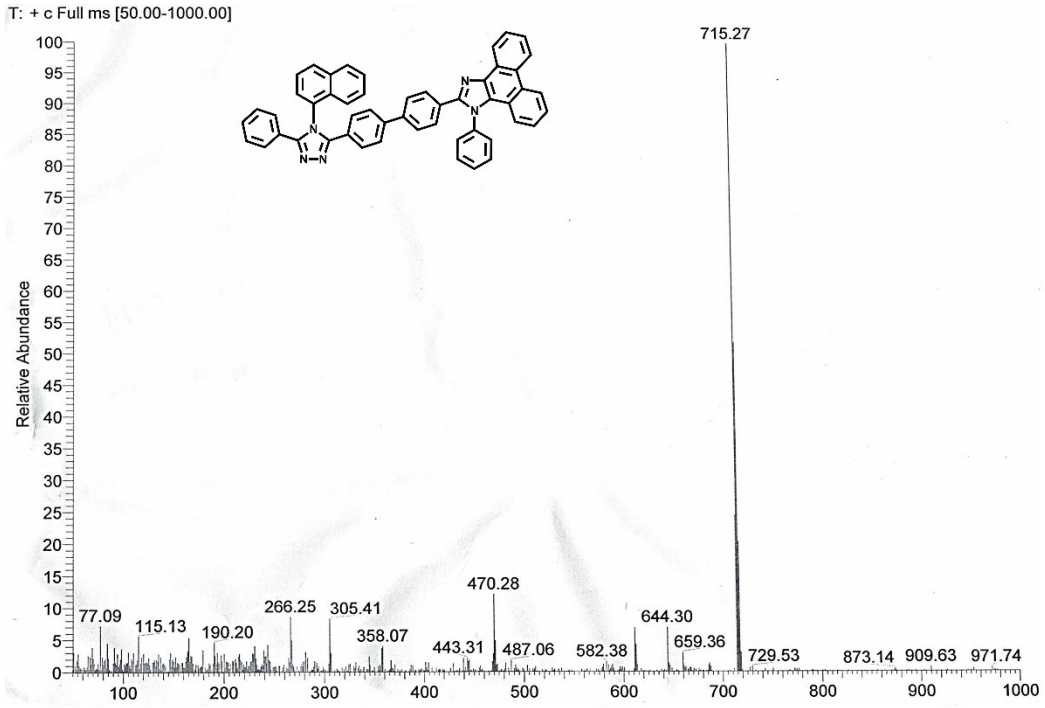

Figure S15. Mass Spectrum of 4NTAZ-PPI.

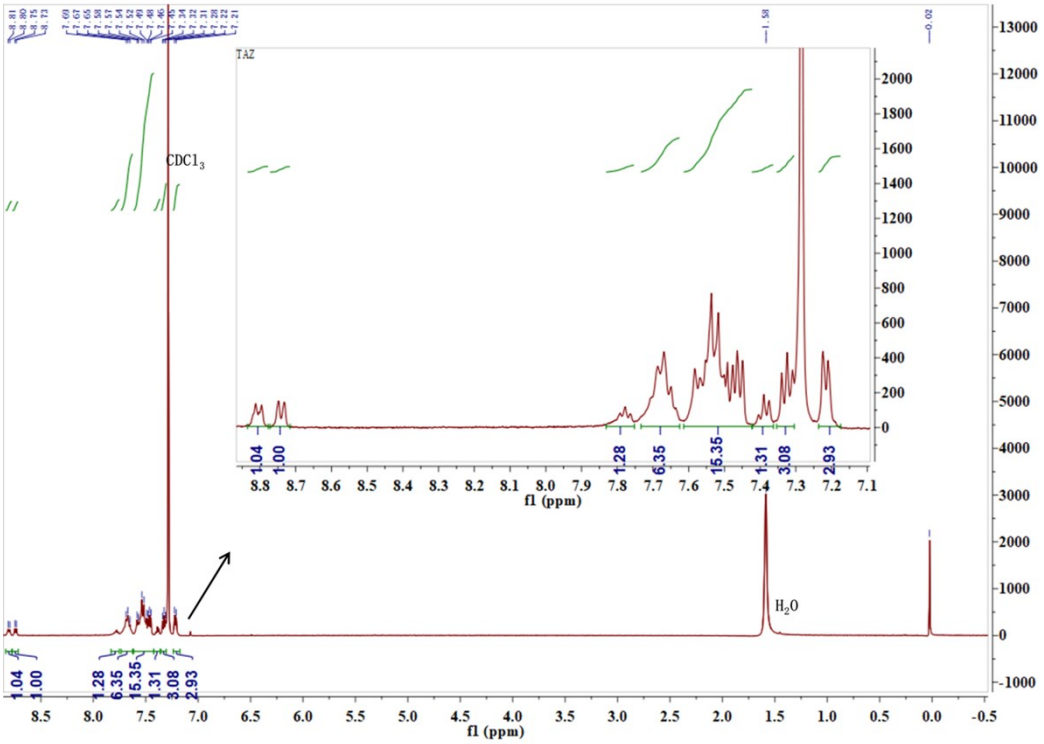

Figure S16. ^{1}H NMR spectrum of TAZ-PPI in $CDCl_3$.

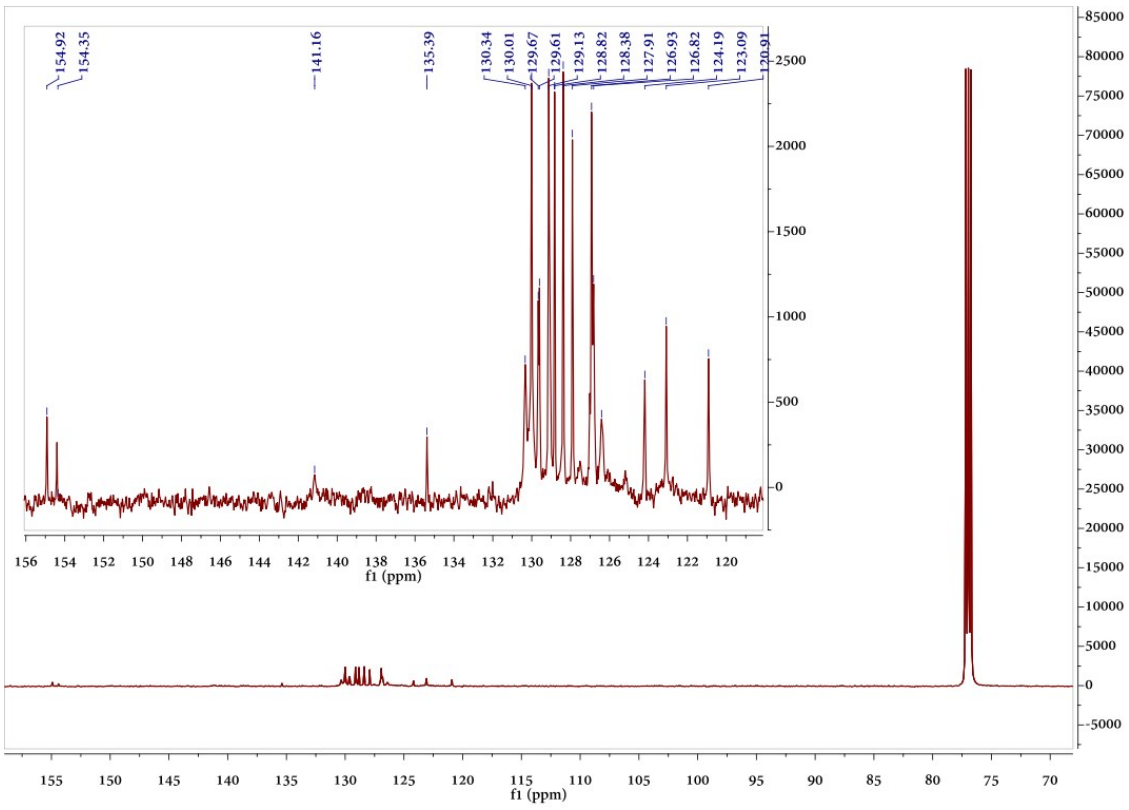

Figure S17. ^{13}C NMR spectrum of TAZ-PPI in $CDCl_3$.

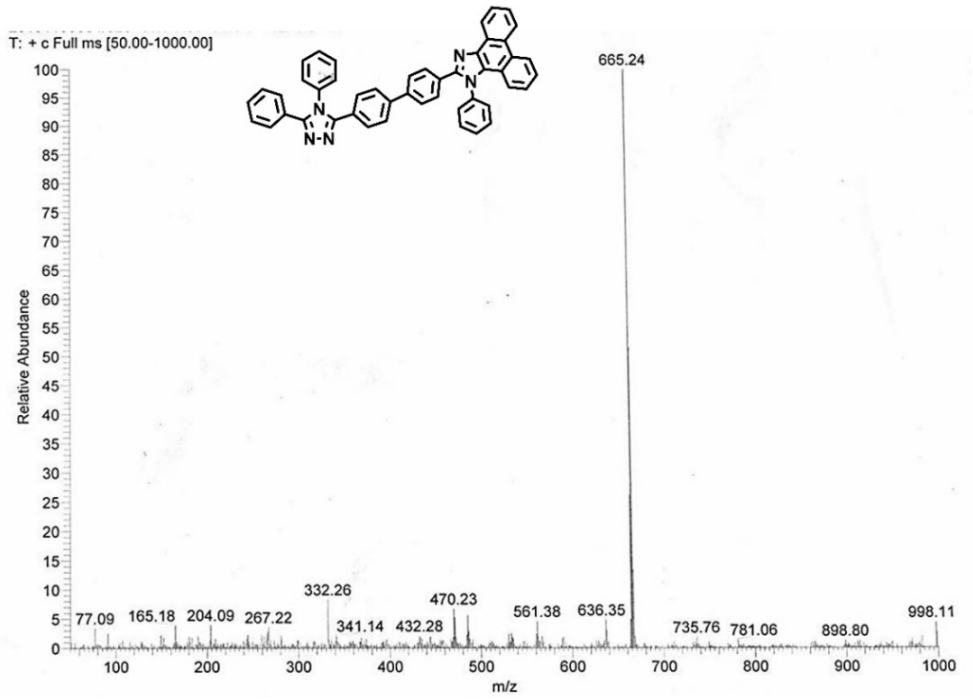

Figure S18. Mass Spectrum of TAZ-PPI.